Chemical Engineering Journal 158 (2010) 305–314

Contents lists available at ScienceDirect

Chemical Engineering Journal

journal homepage: www.elsevier.com/locate/cej

Analysis and optimization of a micromixer with a modified Tesla structure

Shakhawat Hossain, Mubashshir A. Ansari, Afzal Husain, Kwang-Yong Kim *

Department of Mechanical Engineering, Inha University, 253 Yonghyun-Dong Nam-Gu, Incheon 402-751, Republic of Korea

ARTICLE INFO

Article history:
Received 22 August 2009
Received in revised form 12 January 2010
Accepted 2 February 2010

Keywords:
Modified Tesla structure
Coanda effect
Transverse dispersion
Mixing index
Optimization
Surrogate method

ABSTRACT

A flow-analysis method using Navier–Stokes equations has been applied to a parametric study on a micromixer with a modified Tesla structure, and an optimization of this micromixer has been performed with a weighted-average surrogate model based on the PRESS-based-averaging method. The numerical solutions are validated with the available numerical and experimental results. The mixing performance and pressure-drop have been analyzed with two dimensionless parameters, i.e., the ratio of the diffuser gap to the channel width, θ, and the ratio of the curved gap to the channel width, ϕ, for a range of Reynolds numbers from 0.05 to 40. The shape of the microchannel is optimized at the Reynolds number of 40 with two objectives: the mixing index at the exit and the friction factor. The "naïve approach" has been applied to realize a single-objective optimization problem. The optimization results reveal that the mixing and pressure-drop characteristics are very sensitive to the geometric parameters. Sensitivity analysis reveals that in the vicinity of the optimum point, the objective function is more sensitive to ϕ as compared to θ.

1. Introduction

With the trend of the miniaturization of various fluid systems, microfluidic devices, such as micropumps, microvalves, and micromixers, have been intensively researched. Microfluidic-mixing applications have expanded into many fields, including medical-drug delivery and biological, chemical, and thermal applications. The scaling down of fluid systems also raises some new issues, among which the micromixing of fluids is very important. Microfluidic devices have been widely utilized in 'micro-total analysis systems' (μTASs) or lab-on-a-chip systems for biological analysis, chemical synthesis, and clinical purposes. At microscopic scales, fluid mixing becomes very difficult. The dimension of a microfluidic device is typically in the order of sub-millimeters and conventional methods for stirring fluids are not applicable. More importantly, *Re* (the Reynolds number) is small, which means the flow is laminar and the mixing solely depends on molecular diffusion, which is usually very slow. Hence, in many applications, it is necessary to apply specially designed micromixers to promote mixing [1,2].

In order to enhance fluid mixing in microchannels, recently a variety of active and passive micromixers have been developed. Active micromixers depend on external fields to force fluids to mix together inside microchannels [3,4]. Active micromixers generally enhance mixing by stirring the flow in order to create secondary flows. This stirring-effect can be achieved by using additional structures or external sources, including ultrasonic vibration, dielectrophoresis, electrohydrodynamic, electroosmosis, and magnetic-force techniques. The secondary flow stretches and folds the interface of the fluids, thereby reducing the diffusion path between the fluid streams and increasing the mixing phenomenon. However, the fabrication of this type of microfluidic mixer is rather complex. Furthermore, these devices generally require some form of external power sources and control systems. Passive micromixers do not require external energy; the mixing process is governed by modifying the microchannel with different shapes or structures. Passive mixers can be further classified as lamination micromixers and injection micromixers. In lamination mixers, the fluid streams are divided into several small streams, which are later joined in a mixing channel [5]. On the other hand, an injection mixer splits only one stream into many sub-streams in the form of microplumes, which increase the contact surface and reduce the mixing path. In addition, active micromixers are generally more complex and thus, can be difficult to operate, fabricate, clean, and integrate into microfluidic systems. Passive mixers are used in most microfluidic applications. Bessoth et al. [6] reported a passive mixer that reduced the diffusion path between the fluid streams by splitting and recombining the flow.

Hong et al. [7] demonstrated an innovative, passive micromixer that uses the "Coanda effect," which produces transverse dispersion with two-dimensional modified Tesla structures. The Coanda effect, named after Henri-Marie Coanda, who first identified the effect in 1910, involves the tendency of fluids to follow a surface; it can be the defining effect of a jet-flow phenomenon in which a jet attaches itself to a nearby surface and follows that curved surface, away from its initial direction. This structure makes use of the Coanda effect to split the fluid stream and to direct a part

* Corresponding author. Tel.: +82 32 872 3096; fax: +82 32 868 1716.
E-mail address: kykim@inha.ac.kr (K.-Y. Kim).

1385-8947/$ – see front matter © 2010 Elsevier B.V. All rights reserved.
doi:10.1016/j.cej.2010.02.002

Nomenclature

H	curved gap distance (mm)
s	diffuser gap distance (mm)
B	depth of the channel cross-section
D	diffusion coefficient
Lc	axial length of the main channel (mm)
Lo	length of the channel inlet (mm)
Le	length of the channel outlet (mm)
W	width of the channel cross-section (mm)
N	number of sampling points
Re	Reynolds number
M	mixing index
c	mass fraction
F	objective function
w_f	weighting factor
f	friction factor
Δp	pressure-drop

Greek letters

μ	absolute viscosity of fluid (kg m^{-1} s^{-1})
ρ	fluid density (kg m^{-3}).
σ	variance
α, β	exponents for weighted-average models
θ	ratio of the diffuser gap to the channel width
ϕ	ratio of the curved gap to the channel width
λ	aspect ratio of the inlet cross-section

Subscripts

m	mixture
opt	optimum value
i	sampling point
max	maximum value
min	minimum value
x	axial distance (mm)

of the stream so that it recombines with the opposing flow of the other part of the stream. In this structure, the Coanda effect causes chaotic advection and significantly improves mixing. The physical properties of water were applied in the simulation. In the experiments, blue- and yellow-dyed DI (de-ionized) water were used as working fluids.

Asgar et al. [8] analyzed the mixing performance of a modified Tesla structure by both numerical and experimental investigations at a Reynolds number of 0.05. They experimentally observed 78% mixing at 5 mm downstream of the inlet in a 0.1 mm-wide microchannel. In the experiments of Asgar et al. [8], DI water that was fluorescently labeled with Dragon green dye and pure DI water were used as the working fluids. They also reported that experimental and numerical results showed good agreement with a 4% error on average. Hong et al. experimentally observed 72% mixing at a 7 mm distance from the inlet in a 0.2 mm-wide microchannel at $Re = 0.1$ and numerically reported that at the flow rate of 10 ml min^{-1} ($Re < 10$), a modified Tesla structure can achieve full mixing after fluid passes four mixing cell-pairs (which are within a length of approximately 7 mm). They also compared this result for the mixing with a T-type micromixer with the same cross-sectional area.

From the above discussion, it is clear that a modified Tesla structure is effective in enhancing the mixing of fluids by creating transverse dispersion. However, there have not been any reports on systematic investigations to find the effects of geometric parameters on the mixing performance and fluid-flow characteristics in a modified Tesla structure. However, for a staggered herringbone (grooved) micromixer (SHM, for short), Ansari and Kim [9] performed shape optimization by using the response surface method and a three-dimensional Navier–Stokes analysis of the flow. They reported that mixing can be effectively increased by optimizing the shape of the grooves.

In the present work, numerical analysis on mixing in a modified Tesla micromixer has been performed to investigate the variation of the mixing behavior and flow characteristics with geometric parameters for a wide range of the Reynolds number. Shape optimization has also been carried out with two objective functions: the mixing index at the exit and the friction factor. A weighted-average surrogate model is employed as a numerical optimization tool to obtain an optimal structure by considering two geometric design variables. Mixing in the channel has been analyzed through three-dimensional Navier–Stokes equations with two working fluids, viz., water and ethanol. The effects of two design parameters of a modified Tesla structure on the mixing behavior have been investigated at six Reynolds numbers that range from 0.05 to 40.

2. Numerical analysis

A schematic diagram of the modified Tesla geometry is shown in Fig. 1 with three units. The two different fluids, water and ethanol, enter from two inlets, as shown in the figure, and there is an outlet on the right side. The main Tesla channel is joined to the inlets at a T-joint. The width of the channel, W, is kept constant for all repeating units and the remaining part of the main channel. The dimensions are as follows: axial length of main channel (Lc) = 2.37 mm; width of the channel (W) = 0.2 mm; depth of the channel (B) = 0.2 mm; Lo = 0.1 mm; d = 0.175 mm; and Le = 2 mm. Le is the outlet channel length, starting form end of the Tesla units to the outlet. The other dimensions, h and s, vary from 0.03 mm to 0.07 mm and from 0.04 mm to 0.12 mm, respectively, while the total length of the channel is fixed at 4.47 mm, which is the sum of the channel-section lengths, i.e., Lo, Lc, and Le. The aspect ratio of the channel cross-section, W/B, is unity (the width of the channel is the same as the depth). The two inlets, Inlet 1 and Inlet 2, are merged in the main microchannel with a T-joint, as shown in Fig. 1. The properties of water and ethanol have been taken at 20 °C and are listed in Table 1. The diffusivity for both water and ethanol is 1.2×10^{-9} m^2 s^{-1}.

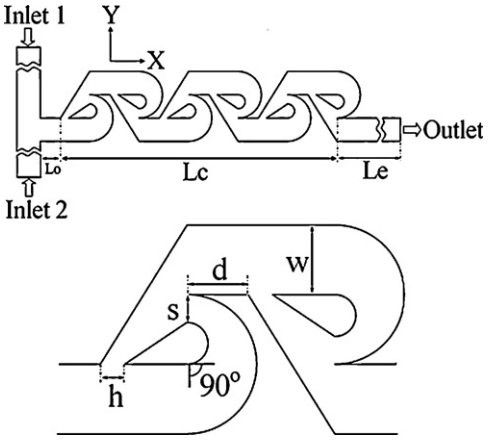

Fig. 1. Schematic diagrams of the modified Tesla structure.

Table 1
Properties of fluids at 20 °C.

Fluid	Density (kg m^{-3})	Viscosity (kg m^{-1} s^{-1})	Diffusivity (m^2 s^{-1})
Water	9.998×10^2	0.9×10^{-3}	1.2×10^{-9}
Ethanol	7.890×10^2	1.2×10^{-3}	1.2×10^{-9}

A commercial CFD (computational fluid dynamics)-code, ANSYS CFX-11.0 [10], has been used to analyze the flow and mixing in the micromixers. The ANSYS CFX-11.0 code solves three-dimensional steady continuity and momentum (Navier–Stokes) equations by using the finite-volume method via a coupled solver. ANSYS CFX is capable of modeling fluid mixtures that comprise many separate physical components, where each component may have a distinct set of physical properties. To calculate the fluid flow, the CFX-solver will calculate the appropriate average values of the properties for each control volume in the flow domain. These values depend on the values of the componential properties and the percentage of each component that is present in the control volume. In the case of multi-component fluids, the fluids are mixed at the molecular level; it is assumed that the properties of the fluids are depending on the proportions of components. It is also assumed that the mass fraction arises through convection and diffusion. The differential motions of the individual components in the mixture are computed by the relative mass flux terms. This term models the effect of concentration gradients, pressure gradients, etc.

An unstructured tetrahedral grid system was created for the full model through ANSYS ICEM 11.0. Navier–Stokes equations in combination with an advection–diffusion model are applied to analyze the actual mixing phenomena. The numerical simulation is not free from numerical diffusion errors, which arise from the discretization of the convection terms in the Navier–Stokes equation. Numerical diffusion cannot be completely ignored; however, it can be minimized by adopting certain techniques [11]. The velocities at the inlets and zero static pressure at the outlet are specified as the boundary conditions. The solutions are considered to have attained convergence when the value of the root-mean-squared (rms) relative residual is at most 10^{-6}.

The mixing efficiency is quantified by calculating the variance of the mixture in the micromixer. To evaluate the degree of mixing in the micromixer, the variance of the mass fraction of the mixture in a cross-section that is normal to the flow direction is defined as follows.

$$\sigma = \sqrt{\frac{1}{N}\sum (c_i - \bar{c}_m)^2}. \quad (1)$$

In the above definition, N is the number of sampling points inside the cross-section, c_i is the mass fraction at sampling point, i, and $\bar{c}_m$ is the optimal mixing mass fraction. To quantitatively analyze the mixing performance of the micromixer, the mixing index is defined as follows:

$$M = 1 - \sqrt{\frac{\sigma^2}{\sigma_{max}^2}}, \quad (2)$$

where σ is the standard deviation of the concentration across the channel in a cross-section at any specific longitudinal location and σ_{max} is the maximum standard deviation (unmixed at the exit). A greater mixing index indicates a higher quality of mixing; thus, the value of this mixing index is 0 for completely separate streams (for which $\sigma = \sigma_{max}$) and 1 for completely mixed streams (for which $\sigma = 0$).

3. Design variables and objective functions

In this work, two different components of the objective function are employed to optimize the modified Tesla structure: one (F_1) is the component that is related to the mixing index at the end of third cell of the micromixer and the other (F_2) is the component that is related to the friction factor (or pressure loss) in the micromixer. The pressure loss is directly related to the pumping power that is required to drive the fluids in the micromixer. The present optimization problem is defined as the minimization of the objective function, $F(x)$, with $x_i^l \le x_i \le x_i^u$, where x_i indicates the ith design variable and x_i^l and x_i^u are the lower and upper bounds, respectively, of the ith design variable. Two design variables, θ and ϕ, are chosen for the optimization, where θ is defined as h/W and ϕ as s/W. Nine experimental points are selected through a three-level, full-factorial design. Table 2 shows these design variables with their ranges, while the other dimensions of the microchannel are kept constant for all cases.

Table 2
Design variables and their ranges.

Design variable	Lower limit	Upper limit
θ (h/W)	0.15	0.35
ϕ (s/W)	0.2	0.6

The weighted sum of objective functions method, which is also known as the "naïve approach" [12], is generally used for multi-objective optimization problems to develop a single-objective function from multiple objectives. By this method, two objectives, F_1 and F_2, are linearly combined with a weighting factor, w_f, to represent a single-objective function, F, as follows:

$$F = F_1 + w_f F_2. \quad (3)$$

The weighting factor, w_f, can be selected as per the design requirements. In this equation, F_1 is defined as:

$$F_1 = \frac{1}{M_e}, \quad (4)$$

where M_e is the mixing index at the end of third cell of the micromixer. The other component that is related to the friction factor is defined as:

$$F_2 = \frac{f}{f_o}. \quad (5)$$

In this equation, the friction factor, f, is defined as:

$$f = \frac{D_h}{2\rho_f u_{avg}^2} \cdot \frac{\Delta p}{L_x}, \quad (6)$$

where D_h is the hydraulic diameter of the channel inlet, Δp is the pressure-drop in the microchannel, ρ_f and u_{avg} are the average density and velocity of the mixing species, respectively, and L_x is the axial length of the channel. Further, f_o (in Eq. (5)) indicates the friction factor for laminar flow in a smooth channel and is evaluated by the following formula [13]:

$$f_o Re = 24(1 - 1.355\lambda + 1.9467\lambda^2 - 1.7012\lambda^3 + 0.9564\lambda^4 - 0.2537\lambda^5), \quad (7)$$

where λ is the aspect ratio of the cross-section of the channel inlet.

The next steps in the optimization are to construct the surrogates and to find the optimal points.

4. Optimization methodology

In the first step of the optimization procedure, the design variables are selected and the design space is decided for improving the system performance. The objective functions are calculated by the three-dimensional Navier–Stokes analysis at the design points (or experimental points), which are selected through the design-of-experiments (DOE) framework. Then, the surrogate model is constructed based on these objective function values. The surrogate methods used in this work are described below.

Generally, optimization algorithms require many evaluations of the objective functions to search for the optimum solutions in the design space. Therefore, to evaluate these objective function values, a surrogate is constructed to avoid experimental or numerical

expense and save computational time. Surrogate-approximation models are used to predict better designs for problems that are computationally and experimentally expensive [14]. A PRESS-based-averaging (PBA) model, which was proposed by Goel et al. [15] (termed as WTA3) as a weighted-average surrogate model, is used in this work. As described below, this model is composed of three basic surrogate models: response surface approximation (RSA); Kriging (KRG); and Radial Basis Neural Network (RBNN).

The RSA model [16], which is a second-order polynomial function, is fitted to get the response surface approximation. The polynomial function has the form:

$$\hat{F} = \beta_0 + \sum_{j=1}^{n} \beta_j x_j + \sum_{j=1}^{n} \beta_{jj} x_j^2 + \sum \sum_{i \neq j}^{n} \beta_{ij} x_i x_j, \tag{8}$$

where the β's are the regression coefficients, n is the number of design variables, and x_i represents the ith design variable ($i = 1, \ldots, n$).

The RBNN [17] is a two-layered network that consists of a hidden layer of radial basis functions and a linear output layer. The radial basis functions act as activation functions; for each of these functions, the response varies between the input and the center. Further, the distance between any two points is established by the difference in their respective coordinates and by the set of parameters. The linear model, f, for the function can be expressed as a linear combination of a set of N basis functions:

$$f(x) = \sum_{j=1}^{N} w_j y_j, \tag{9}$$

where y_j is the jth basis function and w_j is its associated weight. In the present study, a customized RBNN is applied in MATLAB [18] with the help of the function, *newrb*.

The Kriging model [19] is an interpolating meta-modeling technique that employs a trend model, $g(x)$, to capture large-scale variations and $Z(x)$ to capture small-scale variations. Kriging models consist of a global model and localized departures in the following form:

$$\hat{F}(x) = g(x) + Z(x), \tag{10}$$

where $\hat{F}(x)$ is the unknown function of interest, $g(x)$ is the known approximation (usually a polynomial function), and $Z(x)$ represents the localized deviations. $Z(x)$ is the realization of a stochastic process with mean zero and non-zero covariance. The $g(x)$ term is similar to a polynomial response surface, providing a "global" model of the design space. A linear polynomial function is used as the trend model and the systematic-departure terms follow a Gaussian correlation function.

The PBA model [15] is implemented in the present investigation. The predicted response of this model is defined as follows:

$$\hat{F}_{\text{wt.avg}}(x) = \sum_{i}^{N_{\text{SM}}} w_i(x) \hat{F}_i(x), \tag{11}$$

where N_{SM} is the number of basic surrogate models used to construct the weighted-average model. The ith surrogate model at the design point, x, produces a weight, $w_i(x)$, and $\hat{F}_i(x)$ is the response predicted by the ith surrogate model. Weights are carefully selected such that the surrogate that produces a high error has a low error-weight and thus, low contribution to the final weighted-average surrogate, and vice versa. In the present study, a global weight has been selected through the generalized mean-squared cross-validation error (GMSE) or PRESS (in RSA terminology). The weighting method used in the PBA surrogate is given as follows:

$$w_i = \frac{w_i^*}{\sum_i w_i^*}, \tag{12}$$

where

$$w_i^* = (E_i + \alpha E_{\text{avg}})^{\beta} \quad \text{and} \quad E_{\text{avg}} = \sum_{i=1}^{N_{\text{SM}}} \frac{E_i}{N_{\text{SM}}}.$$

The error that is associated with each surrogate is evaluated as:

$$E_i = \sqrt{\text{GMSE}}, \quad i = 1, 2, 3, \ldots, N_{\text{SM}}. \tag{13}$$

Here, the two constants, α and β, are chosen as $\alpha = 0.05$ and $\beta = -1.0$ [15].

By the use of objective function values at the design points, surrogate models are constructed. Eqs. (11) and (12) are used to construct the PBA model. The constructed surrogate is used in searching for the optimal point through the sequential quadratic programming (SQP) feature in MATLAB [18].

5. Results and discussion

A typical flow structure in the modified Tesla micromixer is shown in Fig. 2, which includes the velocity-vector plots for $h/W = 0.15$ and $s/W = 0.2$ at $Re = 40$ on three different x–y planes. The main characteristics of the flow in this modified Tesla micromixer can be defined as follows: one of the fluid streams is split into two streams and then, the two streams combine again and create chaotic advection to enhance the mixing performance. Fig. 2 shows the main stream that enters the unit and is divided into two sub-streams: sub-stream 1 and sub-stream 2, which pass through the diffuser and curved paths, respectively. Velocity vectors are plotted at sections 1, 2, and 3, which are located in the diffuser, curved, and main-exit paths, respectively. The flow patterns at sections 1 and 2 are almost the same, whereby the velocity vectors are parallel to the channel wall everywhere in the cross-section and vortical structures are absent. At section 3, however, the flow can be visualized with a couple of strong, counter-rotating vortices. Thus, in light of the special Coanda effect, the splitting and recombination of the fluid streams enhance the mixing of the fluids.

The results of the parametric study and the design optimization carried out in this work for the modified Tesla micromixer are introduced and discussed in the following sections.

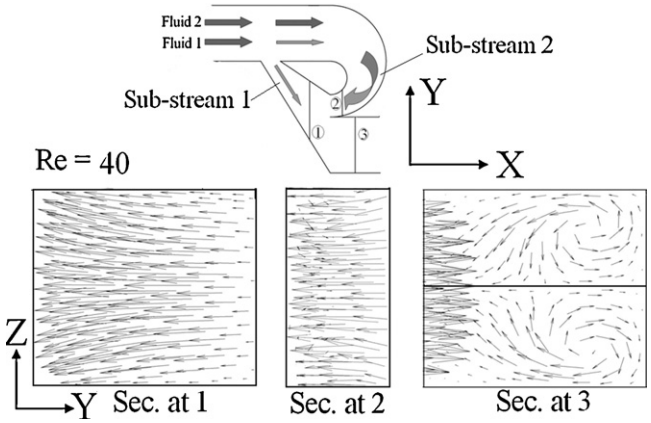

Fig. 2. Velocity-vector plots on yz-planes ($Re = 40$, $h/W = 0.15$, $s/W = 0.2$).

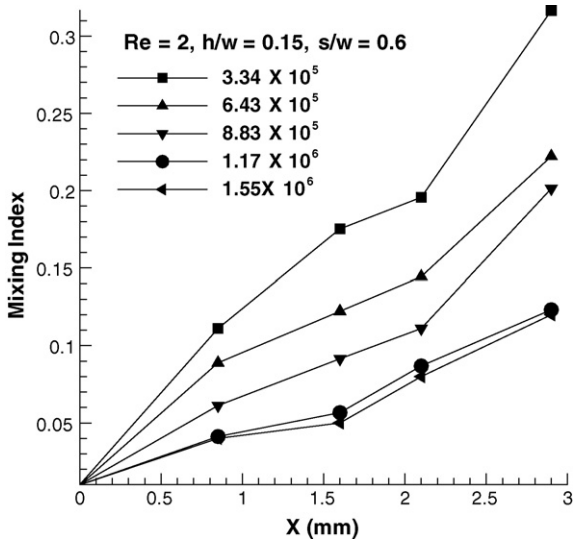

Fig. 3. Grid-dependency test ($Re = 2$, $h/W = 0.15$, $s/W = 0.6$).

5.1. Effects of design parameters

A grid-dependency test has been carried out to find the optimal number of grids and to ensure that the solution is independent of the grid size. As shown in Fig. 3, five different structured grid systems with the number of nodes ranging from 3.34×10^5 to 1.55×10^6 were tested. The distribution of the variance of the mass fraction along the channel was evaluated as the number of nodes was increased. Finally, from the results of the grid-dependency test, the grid system with the number of nodes, 1.17×10^6, was selected as the optimum grid system for further calculations. An example of the unstructured tetrahedral grid system employed in this work is shown in Fig. 4.

In Fig. 5, the present computational results are qualitatively compared with the experimental and numerical results of Asgar et al. [8] for the distribution of the variance, σ_M. As noted in the introductory section, Asgar et al. [8] employed a Reynolds number of 0.05. In this study, the physical properties of water were applied to the two fluids that were considered in the simulation (density, $\rho = 1000\,kg\,m^{-3}$ and dynamic viscosity, $\mu = 10^{-3}\,kg\,m^{-1}\,s^{-1}$). A diffusion coefficient of $D = 10^{-10}\,m^2\,s^{-1}$ was used for the fluids. Experimentally, DI water that is fluorescently labeled with Dragon green dye and pure DI water have been used as working fluids [8]. However, the present numerical calculations used a different pair of working fluids: water and pure ethanol. In this comparison, the present calculation was carried out for the same geometry – with a channel cross-section of ($0.1\,mm \times 0.050\,mm$) – for which Asgar et al. [8] performed numerical calculations and experiments, albeit with slightly different channel dimensions ($0.1\,mm \times 0.055\,mm$). Thus, the differences between the present and previous results shown in Fig. 4 are attributed to these differences in working fluids and geometries. However, the general trend of the present computational results agrees well with those of the previous results.

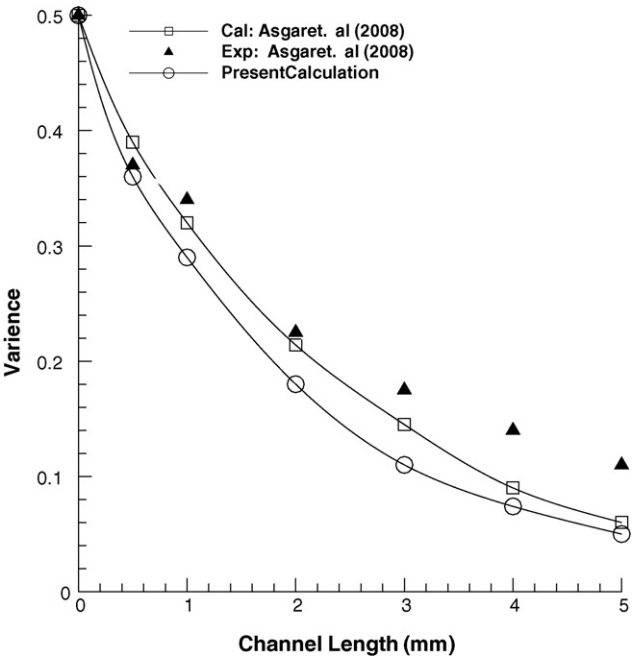

Fig. 5. Comparison of the present numerical results with prior numerical and experimental results (Asgar et al. [8]).

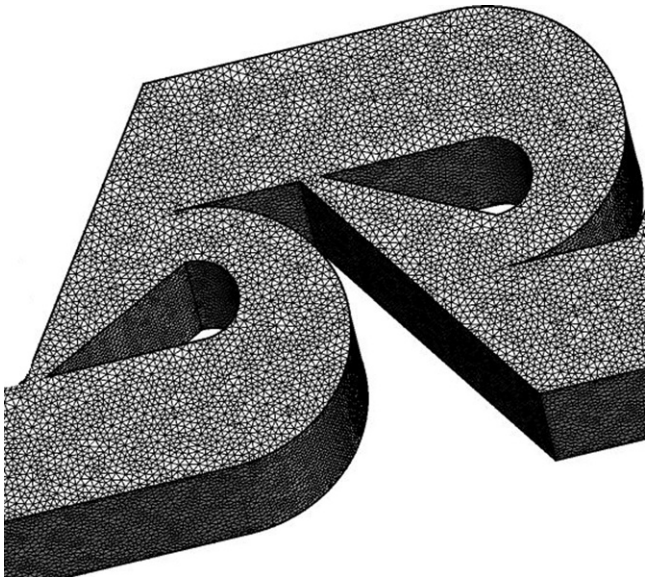

Fig. 4. Example of a structured grid system ($s/W = 0.4$, $h/W = 0.25$).

Fig. 6 shows the effect of the geometric parameter, s/W, on the mixing performance of the modified Tesla micromixer. The mixing indexes are plotted along the channel length in the x-direction for three values of s/W, viz., 0.2, 0.4, and 0.6, as well as for three values of h/W, viz., 0.15, 0.25, and 0.35, at a Reynolds number of 10. The figure has been plotted by evaluating the value of the mixing index on yz-planes after each single unit of the modified Tesla structure. Steep gradients near the inlet of the channel indicate that the two fluids mix rapidly in the initial part of the channel. Beyond a certain length of the channel, the mixing index becomes relatively constant. The mixing performance of the channel improves as s/W decreases. Also, the variation of the mixing index due to s/W decreases over the channel length as h/W increases. Thus, at a higher value of h/W, i.e., 0.35, the mixing is less influenced by s/W, as shown in Fig. 6(c). Furthermore, the gradient of the mixing index in the initial part of the channel increases as s/W decreases.

Fig. 7 shows the variations of the mixing index at the exits of the modified Tesla micromixers with the Reynolds number and s/W. At low Reynolds numbers, the mixing is mainly governed by molecular diffusion and mechanical stirring is ineffective at $Re \ll 1$ [20]. Thus, at a low Reynolds number, i.e., 0.05, the mixing is dominated by the time of residence and depends on the total path of the flow. The values of the mixing index at this low Reynolds number are the same regardless of s/W. As the Reynolds number increases, the

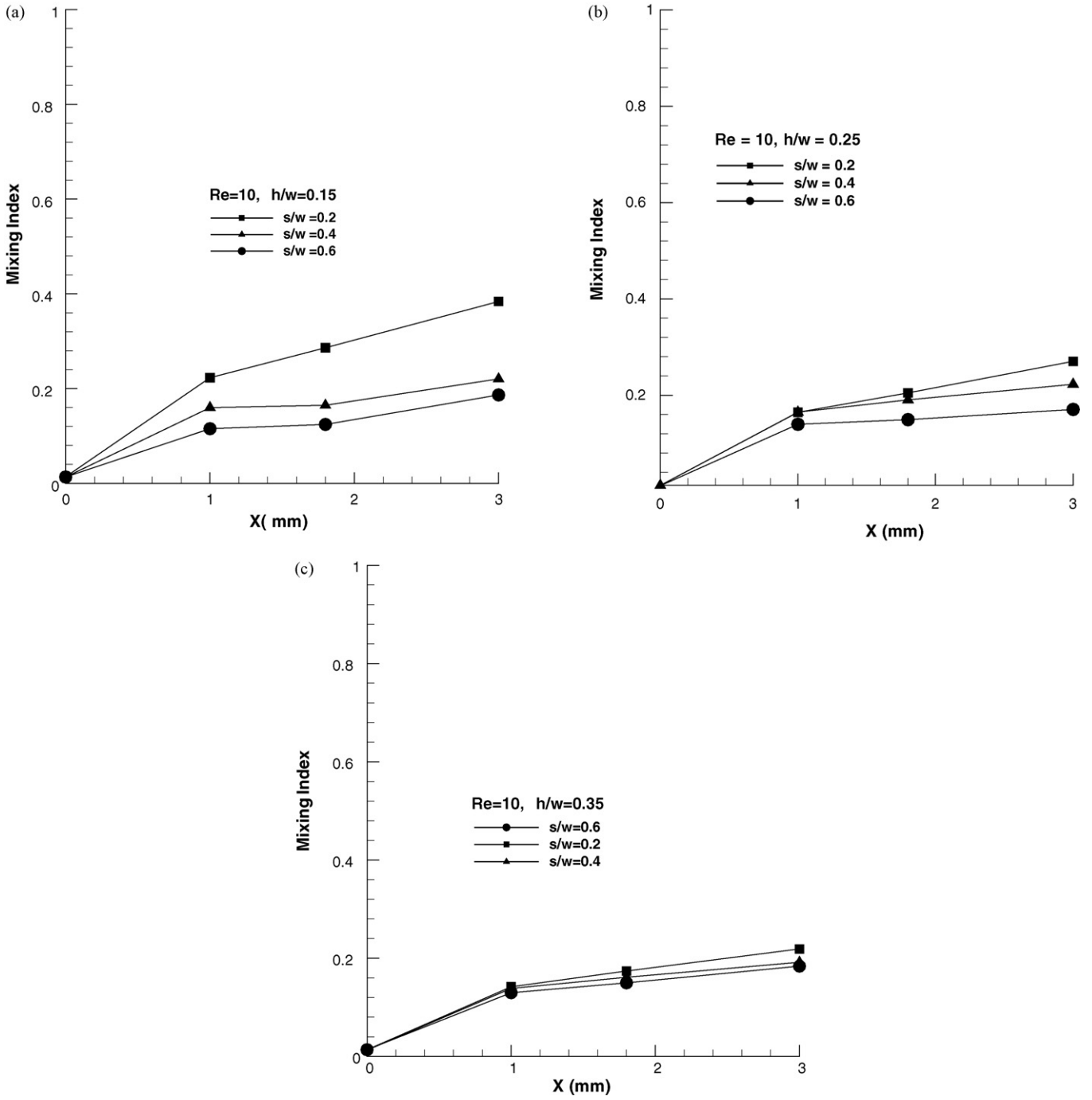

Fig. 6. Effects of s/W on mixing at $Re = 10$: (a) $h/W = 0.15$; (b) $h/W = 0.25$; and (c) $h/W = 0.35$.

level of the mixing index decreases rapidly due to the decrease in the residence time and reaches the minimum at $Re = 2$. Then, the mixing starts to increase with the Reynolds number. For Reynolds numbers around 2, the residence time is insufficient but the transverse flow is still inactive; thus, the mixing index remains at the lower level. However, beyond this level of the Reynolds number, even though the residence time decreases, the transverse flows rapidly become active and mixing starts to increase as the Reynolds number increases. For Reynolds numbers that are larger than 2, the mixing index strongly depends on s/W but the dependency decreases as the Reynolds number increases.

Fig. 8 shows the velocity-vector plots on the yz-plane for a modified Tesla micromixer with $h/W = 0.15$ for various values of s/W at $Re = 2$ and $Re = 40$. When $Re = 2$, the flow pattern is almost the same in every channel, and the velocity vectors are parallel to the channel wall in the cross-section of the channels without any transverse flow. At $Re = 40$, the flow is visualized with the presence of a strong transverse-flow structure, which covers most of the cross-sectional area of the channel. A couple of symmetric, counter-rotating vortices are commonly visualized for the three values of s/W, viz., 0.2, 0.4, and 0.6. This figure also shows that at $Re = 40$, the distance between the centers of these vortices increases with s/W; thus, these centers are shifted to the walls. The pressure-drop characteristics in the modified Tesla microchannel have been analyzed, as they are important in the design of the pump that is needed to drive the flow. Fig. 9(a) and (b) shows the pressure-drop

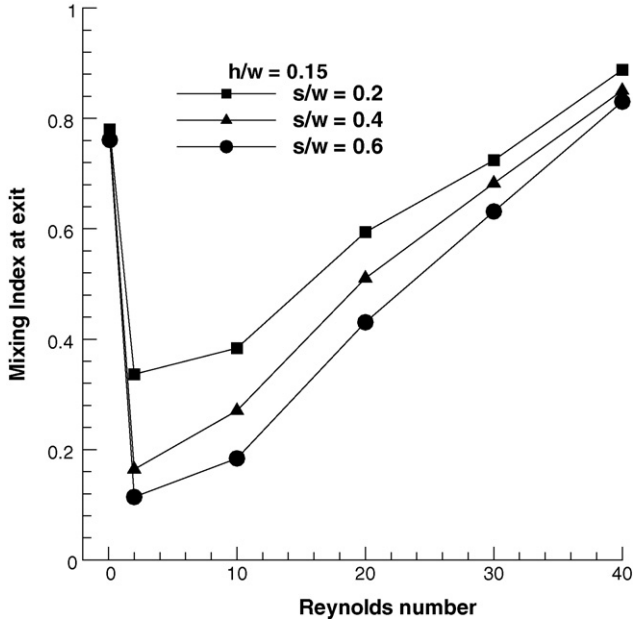

Fig. 7. Variation of the mixing index at the exit with the Reynolds number and s/W at $h/W = 0.15$.

characteristics of the modified Tesla microchannel as a function of the design parameters at various Reynolds numbers. Fig. 9(a) shows the effect of s/W on the pressure-drop at $Re = 10$ for the three values of h/W, namely, 0.15, 0.25, and 0.35. The pressure-drop gradually decreases as s/W increases. For a fixed value of h/W, the rate of decrease in the pressure-drop decreases with s/W. Fig. 9(b) shows the effect of h/W on the pressure-drop, when $s/W = 0.4$, for various Reynolds numbers that range from 0.05 to 40. In all cases, the pressure-drop rapidly increases with the Reynolds number and decreases with h/W. When the Reynolds number is between 0.05 and 10, the pressure-drop is not significantly affected by the value of h/W. However, the effect of h/W becomes pronounced at higher Reynolds numbers, i.e., $Re = 20$, 30, and 40. Fig. 10 shows the pressure-drop characteristics as a function of the Reynolds number for $s/w = 0.4$ and $h/W = 0.15$, 0.25, and 0.35. The pressure-drop

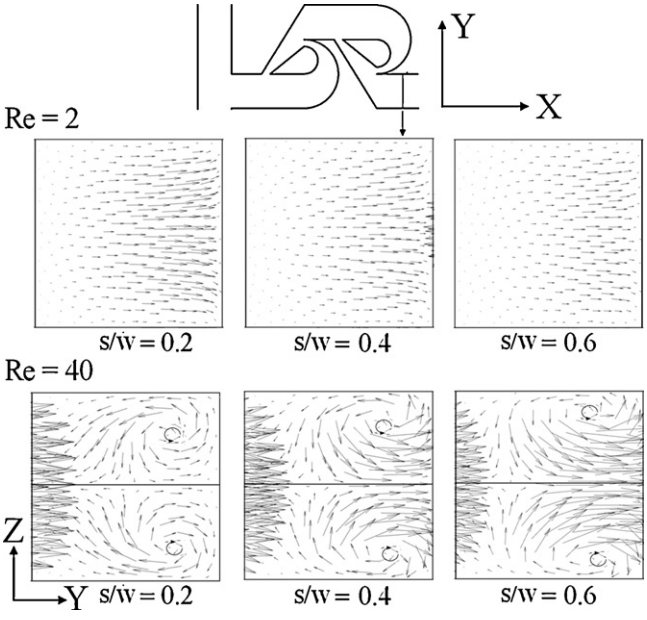

Fig. 8. Velocity-vector plots ($h/W = 0.15$; $Re = 2$ and $Re = 40$).

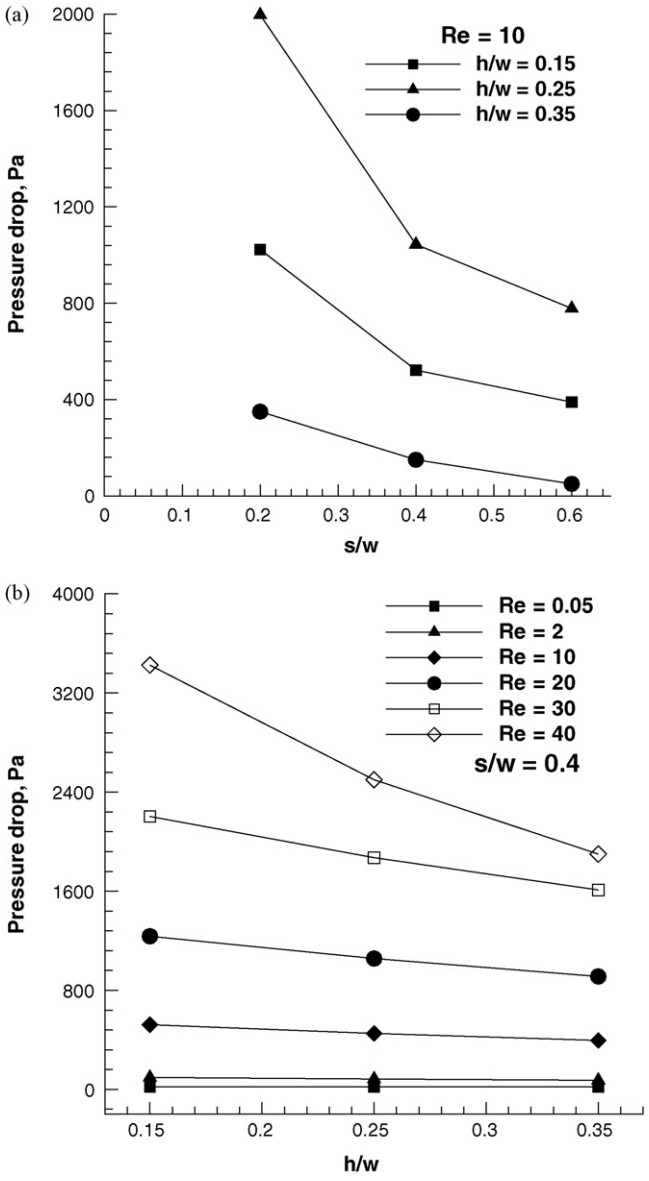

Fig. 9. Effects of geometrical parameters and the Reynolds number on the pressure-drop: (a) s/W at $Re = 10$ and (b) h/W at $s/W = 0.4$.

increases with the Reynolds number for all values of h/W. At lower Reynolds numbers, i.e., $Re = 0.05$ through to 10, where transverse flow is still inactive, the effect of h/W on the pressure-drop is almost negligible. However, at higher values of the Reynolds number ($Re = 20$, 30, and 40), the effect of h/W on the pressure-drop becomes significant. Lower values of h/W induce a higher pressure-drop. Hence, it is clear that the constriction significantly increases the pressure-drop at higher Reynolds numbers, which is disadvantageous as far as the pumping power is concerned.

Fig. 11 shows the mass fraction distributions of ethanol on the yz-plane that is perpendicular to the direction of main flow for $Re = 2$ and 40 at $h/W = 0.15$ and $s/W = 0.2$. At a low Reynolds number, specif., $Re = 2$, a couple of large areas of unmixed fluids are present, and the interface between the two fluids is relatively clear, straight, and less disturbed. This is because at low Reynolds numbers, the inertial force is weak and is unable to create transverse flows in the channel; hence, mixing mainly relies on diffusion. At this Reynolds number (of 2), the value of the mixing index that corresponds to the concentration distribution at the end of the third cell is 0.36. However, as the Reynolds number increases, the area of the interface of

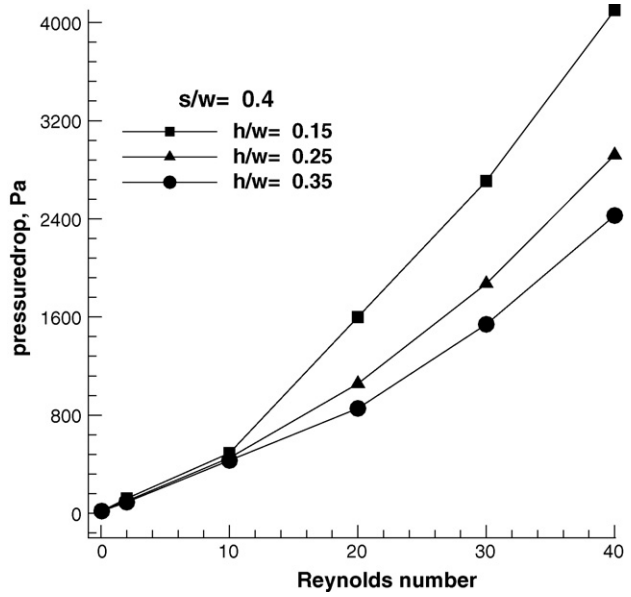

Fig. 10. Variation of the pressure-drop with the Reynolds number at $s/W = 0.4$.

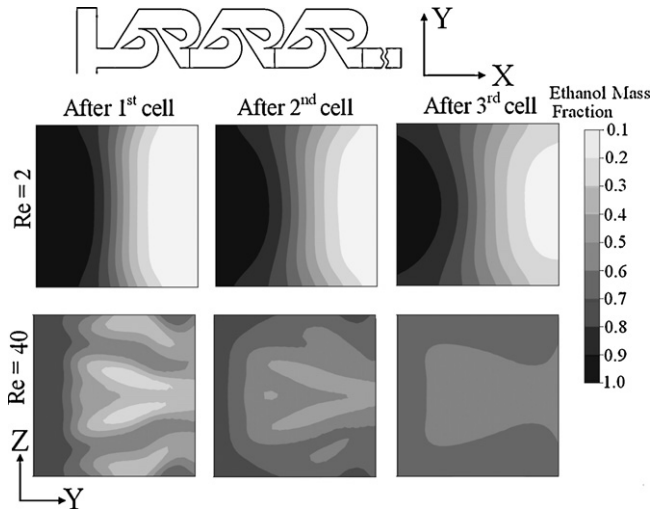

Fig. 11. Concentration distributions of ethanol at various cross-sections ($h/W = 0.15$, $s/W = 0.2$, and $Re = 2$ and $Re = 40$).

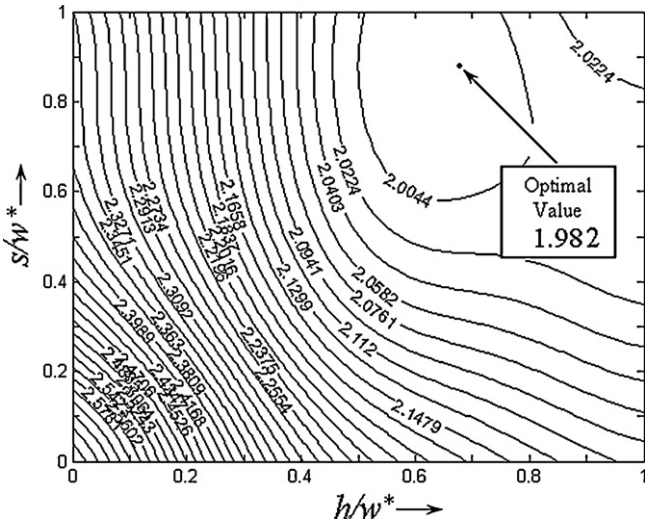

Fig. 12. Contour plot of the objective function.

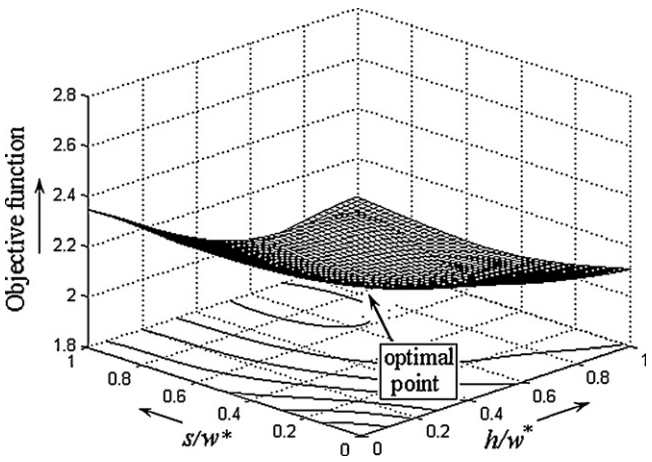

Fig. 13. Surface of the objective function predicted by the PBA model.

the fluids increases, and the mixing is enhanced remarkably, which is due to the development of strong secondary flows. At $Re = 40$, the value of the mixing index that corresponds to the concentration distribution of ethanol at the end of the third cell represents 0.88.

5.2. Design optimization

Shape optimization of the modified Tesla structure has been performed for a composite objective function that consists of the inverse of the mixing index and the friction factor. The optimization has been carried out at a Reynolds number of 40. The mixing index, which is an indicator of the mixing performance, has been inversed for constructing the objective function in the form of minimization. The normalized friction factor has been considered as a component of the objective function, which is an indicator of the pressure loss in the micromixer. In the micromixer, it is necessary to keep the pressure-drop low in view of the low pumping power that is available at the micro-level.

The optimal microfluidic Tesla geometry that is obtained by optimization through the PBA surrogate model has been compared with the reference design, which is chosen arbitrarily from the designs in Table 3. The optimal shape of this micromixer with a weighting factor of 0.05 is found at the design variables, $\theta = 0.32$

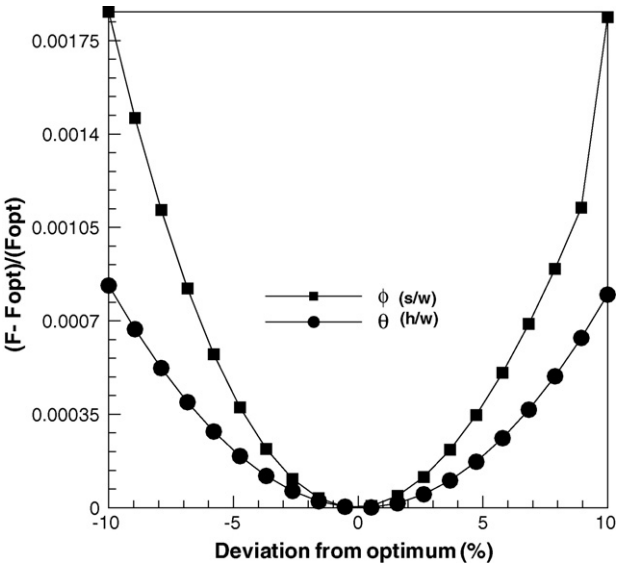

Fig. 14. Sensitivity analysis of the objective function.

Table 3
Results of the optimization with a weighting factor of 0.05.

	Design variables		Mixing index (M_e)	Friction factor (f/f_o)	Objective function (F) $F(x) = 1/M_e + w_f(f/f_o)$
	$\theta(h/w)$	$\phi(s/w)$			
Reference design	0.35	0.20	0.577	12.325	2.349
Optimal design	0.32	0.45	0.702	11.144	1.982

and $\phi = 0.45$. This optimal microfluidic Tesla structure shows a similar mixing index but a lower friction factor as compared to the reference geometry.

Fig. 12 shows the contour plot of the objective function that ensues from the surrogate-based analysis. Horizontal and vertical axes indicate the normalized design variables, h/w^* and s/w^*, respectively. In this figure, the contour lines represent the lines of constant objective function values. Fig. 13 represents the three-dimensional surface plot of the objective function that results from surrogate analysis. It is found in these figures that there is only one local minimum near the upper bound of s/W. The optimal value of 1.982 is obtained at the point (0.647, 0.831).

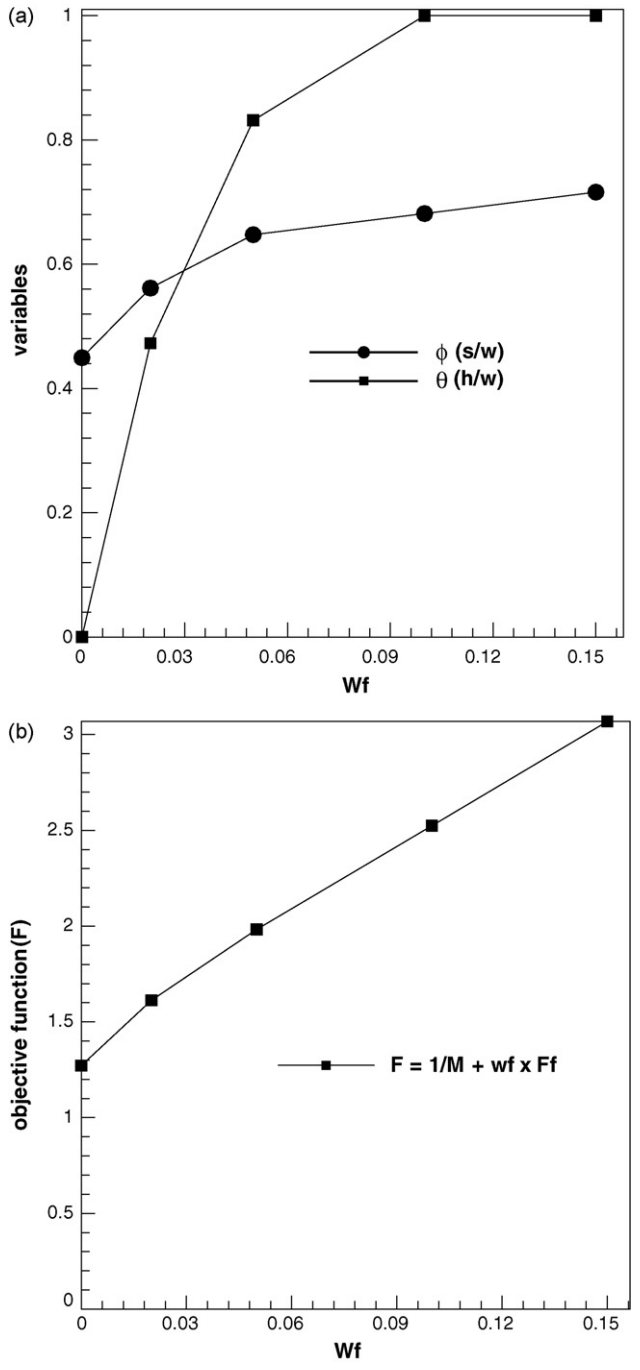

Fig. 15. Variation of the optimization results with the weighting factor: (a) design variables and (b) the objective function.

A sensitivity analysis of the objective function is performed by varying the design variables around the optimal point as shown in Fig. 14. Each design variable is varied from the optimal point in both directions, while the other variables are kept constant. The objective function values at these sets of design variables have been calculated though the surrogate model (PBA). Each design variable varies within ±10% of the optimal value. The sensitivity analysis reveals that the objective function is more sensitive to $\phi(s/w)$ as compared to $\theta(h/w)$ in the specified range.

Fig. 15 shows the results of optimization; the figure represents the variation of the normalized design variables with the weighting factor in the composite objective function. As the weighting factor increases, the values of both the design variables increase. However, the design variable, $\theta(h/w)$, shows a higher rate of increase as compared to $\phi(s/w)$. Fig. 15(b) depicts the variation of the objective function with the weighting factor. This figure shows that the objective function almost linearly increases with the weighting factor.

6. Conclusion

The analysis and optimization of a modified Tesla micromixer have been performed through three-dimensional Navier–Stokes analysis. The mixing and pressure-drop characteristics have been investigated in terms of two geometric parameters, i.e., the ratio of the diffuser gap to the channel width, θ, and the ratio of the curved gap to the channel width, ϕ. The analyses have been carried out for a wide range of the Reynolds number, viz., from 0.05 to 40. The results reveal that the mixing and pressure-drop characteristics are very sensitive to the geometric parameters when the Reynolds number is larger than 2 where secondary flows become active. The results also reveal that less constriction and/or lower values of geometric parameters yield a greater mixing performance as well as pressure-drop. A weighted-average surrogate model, namely, the PBA model, has been applied to the shape optimization of a modified Tesla micromixer at $Re = 40$ with two objectives, the mixing index and the friction factor. The "naïve approach" (of optimizing the weighted sum of objective functions) has been applied to realize a single-objective optimization problem. Through the evaluations of the objective function at nine experimental points that are selected via a three-level full-factorial design, the optimization has been successfully performed to yield optimum designs that strongly depend on the weighting factor that is used in the "naïve approach". Sensitivity analysis shows that the objective function is more sensitive to ϕ as compared to θ near the optimum point.

Acknowledgement

This work was supported by the National Research Foundation of Korea (NRF) grant funded by the Korea government (MEST) (No. 20090083510).

References

[1] N.T. Nguyen, Z. Wu, Micromixers—review, J. Micromech. Microeng. 15 (2005) R1–R16.
[2] D. Erickson, Towards numerical prototyping of labs-on-chip: modeling for integrated microfluidic devices, Microfluid. Nanofluidics 1 (2005) 301–318.
[3] V. Vivek, Y. Zeng, E.S. Kim, Novel acoustic-wave micromixer, in: Proceedings of the IEEE Micro Electro Mech. Syst. (MEMS), 2000, pp. 668–673.
[4] J. Cao, P. Cheng, F.J. Hong, A numerical study of an electrothermal vortex enhanced micromixer, Microfluid. Nanofluidics 5 (2008) 13–21.
[5] D. Gobby, P. Angeli, A. Gavriilidis, Mixing characteristics of T-type microfluidic mixers, J. Micromech. Microeng. 11 (2001) 126–132.
[6] F.G. Bessoth, A.J. Demello, A. Manz, Microstructure for efficient continuous flow mixing, Anal. Commun. 36 (1999) 213–215.
[7] C.C. Hong, J.-W. Choi, C.H. Ahn, A novel in-plane passive microfluidic mixer with modified Tesla structures, Lab Chip 4 (2004) 109–113.
[8] A. Asgar, S. Bhagat, I. Papautsky, Enhancing particle dispersion in a passive planar micromixer using rectangular obstacles, J. Micromech. Microeng. 18 (2008), 085005 (9 pp.).
[9] M.A. Ansari, K.Y. Kim, Shape optimization of a micromixer with staggered herringbone groove, Chem. Eng. Sci. 62 (2007) 6687–6695.
[10] CFX-11.0, Solver Theory, ANSYS, 2007.
[11] S. Hardt, E. Schonfeld, Laminar mixing in different interdigital micromixers: II. Numerical simulations, AIChE J. 49 (2003) 578–584.
[12] Y. Collette, P. Siarry, Multiobjective Optimization: Principles and Case Studies, 1st ed., Springer-Verlag, New York, 2003, p. 45.
[13] R.K. Shah, A.L. London, Laminar Flow Forced Convection in Ducts: A Source Book for Compact Heat Exchanger Analytical Data. Suppl. 1, Academic Press, New York, 1978.
[14] N.V. Queipo, R.T. Haftka, W. Shyy, T. Goel, R. Vaidyanathan, P.K. Tucker, Surrogate-based analysis and optimization, Prog. Aerosp. Sci. 41 (2005) 1–28.
[15] T. Goel, R. Haftka, W. Shyy, N. Queipo, Ensemble of surrogates, Struct. Multidiscip. Optim. 33 (2007) 199–216.
[16] R.H. Myers, D.C. Montgomery, Response Surface Methodology: Process and Product Optimization Using Designed Experiments, Wiley, New York, 1995.
[17] Orr MLG, Centre for Cognitive Science, Edinburgh University, Scotland, 1996. http://anc.ed.ac.uk/rbf/rbf.html.
[18] MATLAB®, The Language of Technical Computing, Release 14, The MathWorks, Inc., 2004.
[19] D.J. Martin, T.W. Simpons, Use of Krining models to approximate deterministic computers models, AIAA J. 43 (2005) 853–863.
[20] H. Wang, P. Iovenitti, E. Harvey, S. Masood, Optimizing layout of obstacles for enhanced mixing in microchannels, Smart Mater. Struct. 11 (2002) 662–667.